J. Fluid Mech. (1993), *vol.* 247, *pp.* 157–177

Stability of a ridge of fluid

By LESLIE M. HOCKING[1] AND MICHAEL J. MIKSIS[2]

[1] Department of Mathematics, University College London, Gower Street, London WC1E 6BT, UK

[2] Department of Engineering Sciences and Applied Mathematics, Northwestern University, Evanston, IL 60208, USA

(Received 23 April 1991 and in revised form 20 July 1992)

The stability and nonlinear evolution of a ridge of fluid on an inclined plane is investigated. This model was introduced by Hocking (1990). Here we present numerical solutions of the model showing the evolution of the ridge and in some cases the formation of droplets. Also, we investigate the linear stability of the fluid ridge allowing for contact-line motion. We find a preferred wavelength for the linear stability of spanwise disturbances.

1. Introduction

The leading edge of a sheet of viscous fluid becomes unstable in the spanwise direction as it flows down an inclined plane. This instability has been illustrated in the experimental work of Huppert (1982). In Huppert's experiments, a fixed volume of fluid was spread evenly across a plane surface and released. The fluid elongated into a thin sheet as the leading edge moved down the plane and when the edge had advanced sufficiently far, it was observed to become unstable. As a result of this instability, one of two possible configurations emerged: either the edge developed long, parallel-sided fingers advancing down the plane with the level where the roots of the fingers were attached to the sheet remaining fixed, or a sawtooth shape developed with both the points and the bases of the triangular protuberances moving downwards. It seems unquestionable that the appearance of this instability must reflect the combined action of gravity and capillarity, and that both of these effects should somehow influence the final configuration of the sheet. Additional experimental work on this problem has been done by Silvi & Dussan V. (1985). They noted in their experiments that the magnitude of the contact angle at the interface could possibly explain the two different observed configurations. By repeating Huppert's experiments with the same fluid but on two different solid surfaces they were able to observe both the fingering and sawtooth configurations. The significant difference between the two experimental situations was the value of the contact angle. Our aim is first to investigate the evolution of the fluid sheet and to determine the effect of the contact angle on its evolution. This will be done by studying a model of a fluid ridge developed by Hocking (1990). Second, we shall investigate the linear stability of a fluid ridge. Here we shall find a critical wavelength of the instability which will be weakly dependent on the slip length of the fluid along the solid.

At the onset of the instability, when the sheet of fluid is thin, capillarity is only a significant factor near the leading edge, with the sheet extending up the slope behind the edge controlled by gravity only. Moreover, analysis of the shape of the profile of the sheet in a vertical plane before the onset of the instability shows the presence of a hump near the edge where the height is considerably larger than in the sheet some

distance up the plane. This suggests that the essence of the physics can be captured by considering the instability of a ridge of fluid with both leading and trailing edges, that is, by ignoring the thin sheet of fluid extending up the plane to the fixed initial position of the fluid at the top of the plane. In any case if a finite volume of fluid is used in the experiment the sheet is essentially a ridge of fluid and we would expect to observe the same instability (and possibly others) here as for the case of a sheet. Hence, independent of the ridge's relationship to the leading edge of a fluid sheet, the motion of a ridge presents an interesting free-boundary problem.

This simpler problem of a fluid ridge and its linear stability to spanwise disturbances was formulated and investigated by Hocking (1990). The basic state consisted of a thin two-dimensional strip of fluid, extending across an inclined plane. The motion was driven by the component of gravity down the plane, and the fluid motion was quasi-static; at each instant there was a balance between the gravitational force and surface tension, and the velocity of the ridge was fixed by the assumptions made concerning the contact angles at the leading and trailing edges of the ridge. These were taken to have a linear variation with velocity, with the excess of the contact angle at the advancing edge above its maximum static value being proportional to the velocity of the edge. A similar relation was assumed for the trailing edge. This procedure holds when the real contact angle as measured at the contact line varies with velocity in a prescribed manner (see, for example, Greenspan 1978); it also holds if this angle is assumed to be fixed, and the variation with velocity refers only to the *apparent* contact angle as measured at some distance from the immediate vicinity of the contact line (Hocking 1981). The latter proposal may be necessary because of a rapid variation in the angle over a small region near the contact line where the standard conditions of the Navier–Stokes boundary conditions may have to be relaxed in order to remove, or account for, a force singularity at the edge itself. The relative merits of these two possibilities are discussed in Hocking (1992). The analysis developed in Hocking (1990) showed that the steady motion with the edges uniform across the span of the flow was unstable to disturbances with a spanwise periodic variation provided that the wavelength of the disturbance was sufficiently large. However, the linear growth rate was found to be an increasing function of the wavelength; with a channel of width d and with maximum or minimum amplitude of the disturbance at the sidewalls, the greatest wavelength that can occur in the channel is $2d$, and then the leading edge will have its maximum displacement at one wall and its minimum at the other, with a monotonic variation between them. This was at variance with the observations of Huppert (1982) for the leading-edge instability of a fluid sheet, for which the wavelength appeared to be independent of the width of the channel.

As no critical wavelength for a channel of infinite width emerged from the linear analysis, it was suggested by Hocking that the selection of a preferred wavelength might come from a nonlinear analysis, and some numerical evidence was obtained to support this claim. More extensive and more soundly based computations have been undertaken, and in the first part of this paper the conclusions reached by these investigations are presented. One major advantage of the ridge problem over the corresponding problem of the extending fluid sheet is that it is easier to extend the calculations to the nonlinear stage.

The linear problem for the leading edge of a fluid sheet has been discussed by Troian *et al.* (1989). They consider the linear stability of the flow near the leading edge of the sheet, where capillarity is an important influence. In their model no contact line is present, but there is a very thin film of fluid extending down the plane

in front of the sheet. The relevant part of the sheet as far as the stability is concerned is the narrow region where the height of the fluid changes from a slowly varying, relatively thick layer to a very thin, almost stationary film. It is this narrow region that is called the leading edge, although there is no edge or contact line present in the flow. Since there is no contact line, contact angles are irrelevant in this model, nor is there any necessity to remove a contact-line stress singularity by slip or some other means, as is essential when a moving contact line is present. Troian *et al.* showed that there was a preferred wavelength for the linear stability of spanwise disturbances to the leading edge, and that this wavelength was only weakly dependent on the thickness of the film ahead of the edge. It is also claimed, though the details are not presented in the paper, that the same conclusion holds for a model with a contact line present. In order to avoid the region close to the contact line, the calculation starts at a position where the height is small but non-zero, and the contact angle there is assumed to be given. Tuck & Schwartz (1990) have also performed some calculations for equations of the same form as those studied by Troian *et al.* for the basic state, that is, without any spanwise variation. In their calculations it is found that the model with a downstream film and that with a contact line yield similar solutions away from the region where the flow merges into the film or the contact line, in the two cases. This is not surprising, since the region at or near contact can be regarded as an inner region of a matched asymptotic expansion, and its function is to provide one boundary condition for the outer flow. The solutions found by Tuck & Schwartz can indeed be made identical by a suitable shift, as they demonstrate.

Since the analysis of Troian *et al.* successfully predicted a preferred wavelength for the linear stability, it is relevant to ask why this was not obtained for the ridge model. In Hocking (1990) it was assumed that the essential influence of the contact-line region could be captured by introducing the contact-angle variation and that the quasi-steady approximation would not significantly influence the stability of the ridge. Such a procedure was not of course adopted by Troian *et al.*, because there was no contact line in their model, though they did include the controlling influence of surface tension in the narrow region where the rapid change in height of the sheet occurred. The second part of this paper examines more closely the ridge model and does not prescribe a contact-angle variation, nor does it involve the quasi-steady approximation. Rather, proper attention is paid to the slip region in the immediate vicinity of the contact line and in which the slope of the fluid can change substantially. The main result of this analysis is that a preferred wavelength can be predicted for the ridge instability, similar to that found by Troian *et al.* for the sheet. This wavelength is weakly dependent on the slip coefficient, which is the ratio of the slip length to the height of the ridge. Since this height depends on the contact angle, the preferred wavelength is also weakly dependent on the contact angle. As a limiting case, we can recover the results of Hocking's (1990) analysis, which was based on an assumed contact-angle variation outside the slip region and the quasi-steady approximation, but this agreement can only be achieved when the slip coefficient is implausibly small. The conclusion is that, for the fluid ridge, there is a preferred wavelength for the linear stability, but it is ill-defined since it is weakly dependent on the (unknown) slip coefficient. A similar imprecision mars the conclusions of Troian *et al.*, since in their case, there is a weak dependence on the (unknown) height of the film ahead of the bulk motion.

2. The equation for the ridge

The equation for the height h of the fluid in the ridge was obtained in Hocking (1990) (hereafter referred to as I). If x and y are non-dimensional coordinates (see figure 1), measured down the plane and horizontally, respectively, and if t is the non-dimensional time, the equation for the non-dimensional height h of the fluid in the ridge can be written in the form

$$\frac{\partial h}{\partial t}+\frac{\partial}{\partial x}\left[h^2(h+\lambda)\left(\frac{\partial}{\partial x}\nabla^2 h+K\right)\right]+\frac{\partial}{\partial y}\left[h^2(h+\lambda)\frac{\partial}{\partial y}\nabla^2 h\right]=0. \tag{2.1}$$

The dimensional quantities x', y', h', λ' and t' are defined by

$$x'=a_0 x, \quad y'=a_0 y, \quad h'=a_0\alpha_0 h, \quad \lambda'=a_0\alpha_0\lambda, \quad t'=(3\mu a_0/\gamma\alpha_0^3)\,t, \tag{2.2}$$

where γ is the surface tension, μ the viscosity of the fluid and λ' the slip length. The parameter $\alpha_0 \ll 1$ is a typical value of the contact angle and so is a measure of the slenderness of the ridge. If the volume of fluid in a width d' of the ridge is equal to V', then the non-dimensional volume V is related to the lengthscale a_0 and the slenderness parameter α_0 by

$$V'=\tfrac{4}{3}Va_0^2 d'\alpha_0, \tag{2.3}$$

and the spanwise width of the ridge $d'=a_0 d$. The effect of the component of gravity down the plane is measured by the parameter K, defined by

$$K=\frac{\rho g\sin\theta a_0^2}{\gamma\alpha_0}, \tag{2.4}$$

where g is gravity and θ is the angle of slope of the plane. The positions of the leading and trailing edges are given by

$$x=a(y,t), \quad x=b(y,t), \tag{2.5}$$

and the boundary conditions are that

$$\left.\begin{aligned} h&=0 \quad \text{at} \quad x=a,b,\\ \frac{\partial h}{\partial y}=0, \quad \frac{\partial^3 h}{\partial y^3}&=0 \quad \text{at} \quad y=0,d. \end{aligned}\right\} \tag{2.6}$$

The last pair of conditions are appropriate for a periodic solution with wavelength $2d$ in the spanwise direction; alternatively they reflect the presence of sidewalls to the ridge across which no fluid can pass (the presence of boundary layers on these sidewalls is ignored). The condition that the total volume of fluid in the ridge remains constant can be written in the form

$$\int_0^d\int_b^a h\,\mathrm{d}x\,\mathrm{d}y=\tfrac{4}{3}dV. \tag{2.7}$$

The final set of conditions needed to specify the problem relates to the assumptions made about the contact angle at the two edges. It takes a different form in each of the two problems to be studied and will be defined precisely in the relevant section. The lengthscale a_0 has not yet been specified, and a suitable choice can eliminate one of the parameters K or V.

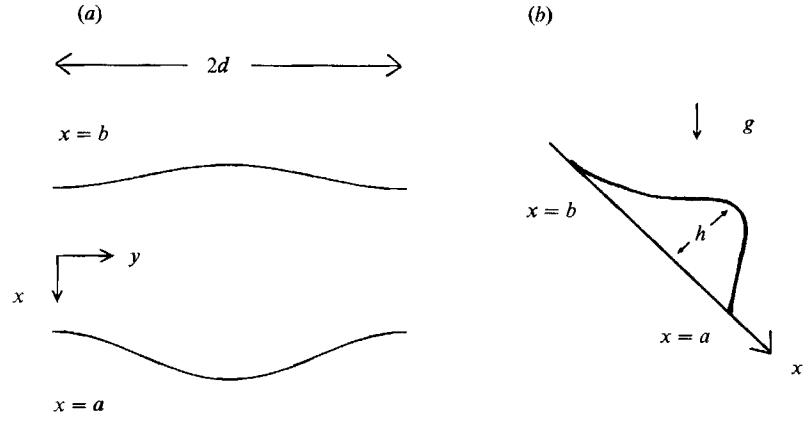

FIGURE 1. (*a*) Periodic ridge of fluid of period $2d$ and volume $2V$, plan view. (*b*) Vertical cross-section of the ridge of fluid moving down the plane.

3. Numerical solution of the ridge with given contact-angle behaviour

Most of the investigations of contact-line motion have been analytical using asymptotic methods. Part of the reason for this is the difficulty involved with a numerical solution due to the sensitivity of the evolution of the interface to the dynamics in the neighbourhood of the contact line. Another reason is that there is not general agreement on the correct slip model for contact-line motion. Most of the numerical work to date (see Greenspan & McCay 1981; Hocking 1981; Haley & Miksis 1991) has been directed to the lubrication model of an axisymmetric or two-dimensional droplet. An interesting limit of the lubrication equations occurs for small capillary number (a different scaling is required to see this explicitly where the characteristic speed is defined by the constant of proportionality in the contact-angle/slip-velocity relationship, see the above references). Here the motion becomes quasi-steady and for both two-dimensional and axisymmetric droplets, the evolution equations reduce to nonlinear ordinary differential equations. At leading order in the capillary number, the slip coefficient does not appear and hence the dynamics is governed by the assumed contact-angle variation at the contact line. A similar limit can be applied to the ridge model (2.1), (2.5)–(2.7) and the result is the model studied in I. Here we shall investigate numerical and analytical solutions of these equations.

Let us begin by defining the lengthscale by the equation

$$a_0^2 = \frac{6\gamma\alpha_0}{\rho g \sin\theta'}, \tag{3.1}$$

so that, from (2.4), $K = 6$. The motion is initiated by making a small change in the position of the leading and/or training edges from a steady position with straight edges and no spanwise variation in h. The time-development of the leading and trailing edges is governed entirely by the assumed contact-angle behaviour. Hence we will assume as in I that the profile of the ridge is quasi-steady and is governed at all times by the balance between gravity and surface tension. Therefore a solution of (2.1) can be found from the simplified form

$$\frac{\partial}{\partial x}\nabla^2 h + 6 = 0. \tag{3.2}$$

This equation is to be solved in the region $b \leqslant x \leqslant a$, $0 \leqslant y \leqslant d$, with boundary conditions (2.6) and the volume constraint (2.7).

Allowing for contact-angle hysteresis, suppose we assume that the maximum and minimum static contact angles are given by $\alpha\alpha_0$ and $\beta\alpha_0$, respectively. Following I, we also assume that, when the contact line is advancing, the contact angle increases linearly with the component of the velocity of the contact line normal to the edge. At a retreating contact line it was assumed in I that the contact angle decreases at the same rate. Here we will assume that the contact angle decreases at a rate proportional to β times the hyperbolic tangent of the slip velocity divided by β. For small velocities this is identical to the linear law but it has the advantage that as the magnitude of the velocity increases, the contact angle is always positive and tends to zero. The linear law is not applicable for velocities so large that a negative contact angle would be implied. Denote the interfaces $x = a$ and $x = b$ as C_a and C_b respectively. Because time only enters the problem through the contact-angle variation, we can redefine the timescale so that, when the edge at C_a is advancing, $\partial a/\partial t$ is positive and the contact angle θ_a along this edge is given by

$$\theta_a = -\frac{\partial h}{\partial x}\bigg|_{x=a}\left[1+\left(\frac{\partial a}{\partial y}\right)^2\right]^{\frac{1}{2}} = \alpha+\frac{\partial a}{\partial t}\left[1+\left(\frac{\partial a}{\partial y}\right)^2\right]^{-\frac{1}{2}}. \tag{3.3}$$

Here we have used the small-angle assumption to replace $\tan(\theta_a)$ by θ_a. Similarly, when the trailing edge C_b is moving down the plane, $\partial b/\partial t$ is positive and the contact angle θ_b is given by

$$\theta_b = \frac{\partial h}{\partial x}\bigg|_{x=b}\left[1+\left(\frac{\partial b}{\partial y}\right)^2\right]^{\frac{1}{2}} = \beta-\beta\tanh\left\{\frac{\partial b}{\partial t}\left[1+\left(\frac{\partial b}{\partial y}\right)^2\right]^{-\frac{1}{2}}\beta^{-1}\right\}. \tag{3.4}$$

For the cases where C_a or C_b is moving up the plane, i.e. the interface at $x = a$ is retreating or the interface at $x = b$ is advancing, the obvious modifications of (3.3) and (3.4) must be made. When the edges are not moving, the contact angles can take any values between β and α. If there is no contact-angle hysteresis, $\beta = \alpha$.

Before we discuss the numerical solution of these equations, let us consider the limit where the lengthscale in the spanwise, y, direction is much larger than the lengthscale in the x-direction. This implies that at leading order (3.2) reduces to an ordinary differential equation in x, for the height h. Solving this equation and applying the boundary conditions (2.6) along C_a and C_b, we find

$$h(x,y,t) = (x-a)(x-b)(2a-b-C-x). \tag{3.5}$$

Here C is a function of t and is defined by using (3.5) in the volume constraint (2.7)

$$C(t) = \frac{8dV+\frac{3}{2}\int_0^d (a-b)^4\,\mathrm{d}y}{\int_0^d (a-b)^3\,\mathrm{d}y} \tag{3.6}$$

Assume that there is no hysteresis and hence set $\beta = \alpha$. Substituting (3.5) into (3.3) and (3.4), assuming a linear contact-angle variation in the retreating case, keeping only leading-order terms and then subtracting the results we find

$$\partial A/\partial t = -2\alpha+\tfrac{1}{3}C^2-3(A-\tfrac{1}{3}C)^2. \tag{3.7}$$

Here we have set $A = a-b$. Note that there is an implicit dependence on y in the above differential equation because the initial values of a and b have a spanwise

variation. Also note from (3.6) that for any reasonable initial data C must be positive. Whenever $C^2 < 6\alpha$, it follows from (3.7) that A decreases with time and will become zero at a finite time at some values of y. Hence a must equal b at some finite time and the ridge will break up into a series of droplets. Whenever $C^2 > 6\alpha$, $\partial A/\partial t < 0$ for A sufficiently small and droplets will again form. For larger initial values of A, it follows from (3.7) that A will approach a constant positive value as $t \to \infty$ provided $C(t)$ tends to a constant. In this limit there will be no spanwise variation and (3.6) and (3.7) show that

$$C = \frac{8V + \frac{3}{2}A^4}{A^3}, \quad 2AC - 3A^2 = 2\alpha, \tag{3.8}$$

and so $A^2 = 8V/\alpha$. We will see that the numerical results predict a similar behaviour. Also note that in I a linear stability analysis of the ridge problem was done and conditions for stability and instability were determined with similar conclusions. This behaviour is in some sense similar to the experimental results of Silvi & Dussan V. (1985). They allowed the same fluid to flow down planes made of different materials. On the plane with the larger static contact angle, fingers formed, while on the other plane with the smaller static contact angle, a coating sawtooth interface developed. There is perhaps some analogy between the droplets in the ridge model and the finger formation and between the uniform ridge and the sawtooth interface. In the former case the plane is not coated and in the second case it is.

A solution with no spanwise variation exists, see I, i.e. $h = h(x, t)$. If we again assume a linear dependence of the contact angle on the slip velocity and set $\alpha = \beta$, we find from (2.6), (2.7) and (3.2)–(3.4) that A is governed by the differential equation,

$$\frac{\mathrm{d}A}{\mathrm{d}t} = \frac{16V}{A^2} - 2\alpha. \tag{3.9}$$

A solution of this equation can be written implicitly as

$$A_0 - A - \tfrac{1}{2}A_\infty \ln\left[\frac{(A - A_\infty)}{(A + A_\infty)}\frac{(A_0 + A_\infty)}{(A_0 - A_\infty)}\right] = 2\alpha t. \tag{3.10}$$

Here we define $A_\infty^2 = 8V/\alpha$ and A_0 is the initial value of A at $t = 0$. We note that as $t \to \infty$ then $A \to A_\infty$. A differential equation for each of the interfaces C_a and C_b separately can also be identified. In I a linear stability analysis of the motion of the ridge about $A = A_\infty$ and governed by (3.9) was done. The result was that if $Q = \pi A_\infty/2d > 1.9987$, then the ridge is linearly stable and if $Q < 1.1997$ then the ridge is linearly unstable (see I for a more general statement of linear stability). We will show shortly that this linear condition for stability approximately holds in the nonlinear case. In particular, we will find that a stable situation corresponds to the ridge with some initial perturbation evolving into a ridge with no spanwise variation, while the unstable case corresponds to the formation of droplets.

In order to solve (3.2)–(3.4) numerically we first need to specify the initial conditions. Suppose that the position of the ridge for $t < 0$ is such that $a = 1$ and $b = -1$. Hence the solution of (3.2) is then

$$h = x - x^3 + V(1 - x^2). \tag{3.11}$$

The slope at the lower edge is equal to $2(V+1)$ and that at the upper edge is equal to $2(V-1)$, and we must have $V \geqslant 1$ for h to be positive between the two edges. At $t = 0$ this solution is perturbed by changing the position of one or both of the edges.

The solution is advanced by solving (3.2) for h with a and b known, from which the positions of each edge at any spanwise location can be determined according to the conditions (3.3) and (3.4) if the slope lies outside the range from β to α, or by keeping them fixed if the slope lies inside this range. These two steps are repeated alternately and the evolution of the edge positions can thus be determined.

For given initial values of C_a and C_b we can determine a numerical solution of (3.2) by using a boundary integral method. First introduce the two functions h_1 and h_2 as

$$h = h_1 - x^3 + c(t)\,(h_2 - x^2). \tag{3.12}$$

Then h will satisfy (3.2) plus the boundary conditions (2.6) if we define $h_i, i = 1, 2$ as

$$\nabla^2 h_i = 0, \tag{3.13}$$

with the boundary conditions

$$h_i = \begin{cases} a^{4-i} & \text{on} \quad x = a \\ b^{4-i} & \text{on} \quad x = b \end{cases} \tag{3.14}$$

for $i = 1, 2$. The time-dependent function $c(t)$ is determined by substituting (3.12) into the volume constraint (2.7)

$$c(t) = \frac{\frac{4}{3}dV + \frac{1}{4}\int_0^d (a^4 - b^4)\,\mathrm{d}y - \iint_S h_1\,\mathrm{d}S}{\iint_S h_2\,\mathrm{d}S - \frac{1}{3}\int_0^d (a^3 - b^3)\,\mathrm{d}y}.$$

This can be rewritten as

$$c(t) = \frac{\frac{4}{3}dV - \frac{3}{4}\int_0^d (a^4 - b^4)\,\mathrm{d}y - \frac{1}{2}\int_{C_a} a^2 \frac{\partial h_1}{\partial n}\,\mathrm{d}s - \frac{1}{2}\int_{C_b} b^2 \frac{\partial h_1}{\partial n}\,\mathrm{d}s}{\frac{1}{2}\int_{C_b} b^2 \frac{\partial h_2}{\partial n}\,\mathrm{d}s - \frac{1}{2}\int_{C_a} a^2 \frac{\partial h_2}{\partial n}\,\mathrm{d}s + \frac{2}{3}\int_0^d (a^3 - b^3)\,\mathrm{d}y}, \tag{3.15}$$

where the region S is one half of a period of the wetted region in the (x, y)-plane, i.e. $S = \{(x, y) : b \leqslant x \leqslant a \text{ and } 0 \leqslant y \leqslant d\}$ and s is arclength. Here we denote the normal partial derivative of h as $\partial h/\partial n$.

We look for periodic solutions of (3.13) of period $2d$ in y. This can easily be done with a boundary integral method by introducing the periodic Green's function of Laplace's equation

$$G(x, y) = (1/4\pi) \ln [\sin^2(\pi y/d) \cosh^2(\pi x/d) + \cos^2(\pi y/d) \sinh^2(\pi x/d)], \tag{3.16}$$

and then using Green's theorem for the value of h_i on the two interfaces. This gives the equation

$$\tfrac{1}{2} h_i(x, y) = \int_{C_a \cup C_b} \left[h_i(\bar{x}, \bar{y}) \frac{\partial G}{\partial n}(x - \bar{x}, y - \bar{y}) - G(x - \bar{x}, y - \bar{y}) \frac{\partial h_i}{\partial n}(\bar{x}, \bar{y}) \right] \mathrm{d}\bar{s}, \tag{3.17}$$

where the line integral is along the two interfaces C_a and C_b and the values of x and y are also along these two interfaces. Discretizing (3.17) results in a linear system of equations for the values of $\partial h/\partial n$ along the two interfaces. Here we used a discretization of the integrals and treatment of the singularities similar to that presented in Miksis, Vanden-Broeck & Keller (1981). Once $\partial h/\partial n$ is determined we can determine the value of $c(t)$ by (3.15) and then update the interfaces by

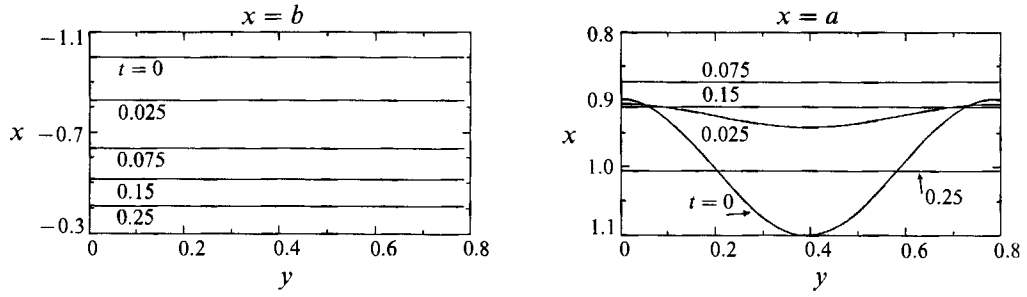

FIGURE 2. The bottom, $x = b$, and top, $x = a$, ridge interfaces at $t = 0$, 0.025, 0.075, 0.15, 0.25 for $\hat{A} = 0.1$, $\alpha = \beta = 10$, $V = 2.5$ and $d = \frac{1}{8}\pi$.

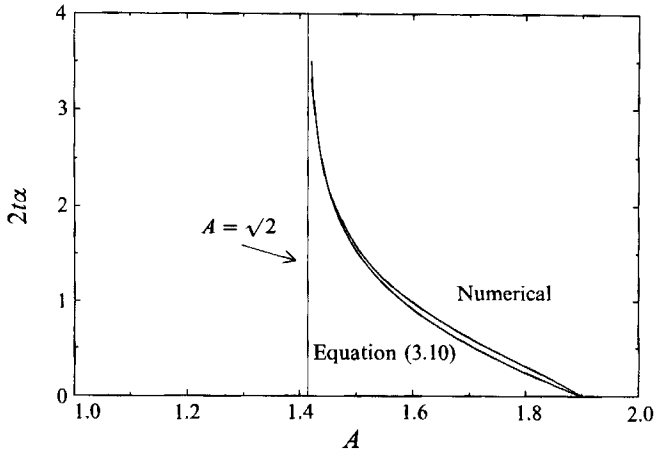

FIGURE 3. A versus t from (3.10) and the numerical results of figure 2 at $y = 0$.

discretizing the slip-velocity/contact-angle relationships (3.3) and (3.4) with a forward Euler method in time. We have found that in several cases a smoothing was required and hence following Longuet-Higgins & Cokelet (1976) a smoothing of the normal derivatives of h along the two interfaces was applied. All spatial integrations were made second-order accurate while the time step was first-order accurate. Care in selecting the space and time steps was necessary in the droplet formation cases since the curvatures in the neighbourhood of the pinching-off points was large compared to the rest of the interface. Also we should note that when hysteresis was present care in selecting the time and space steps was also necessary since the hysteresis resulted in a discontinuous behaviour of the acceleration. The choices for the time and space steps presented here were all found by experimentation and graphical accuracy is present for all the cases discussed.

As initial data for our problem suppose we assume that the interface C_b is always the straight line $x = -1$ while the interface C_a is determined by

$$x = 1 - \hat{A}\cos(\pi x/d). \tag{3.18}$$

Here $\hat{A}$ is the amplitude of the initial perturbation. Our plan is to examine several cases with different values of the parameters. Suppose we set $\hat{A} = 0.1$, $\alpha = \beta = 10$, $V = 2.5$ and $d = \frac{1}{8}\pi$. Note that there is no contact-angle hysteresis for this case. In figure 2 we sketch the initial data plus the interfaces C_a and C_b as functions of time. Here the system (3.2)–(3.4) and (3.15) was solved up to time $t = 0.25$. Note that C_b

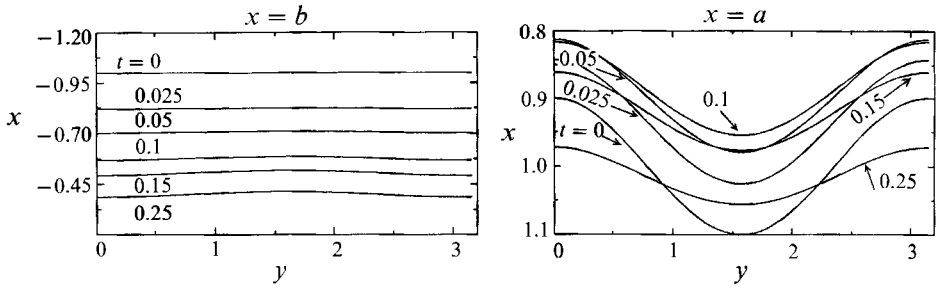

FIGURE 4. The bottom, $x = b$, and top, $x = a$, ridge interfaces at $t = 0$, 0.025, 0.5, 0.1, 0.15, 0.25 for $\hat{A} = 0.1$, $\alpha = \beta = 10$, $V = 2.5$ and $d = \frac{1}{2}\pi$.

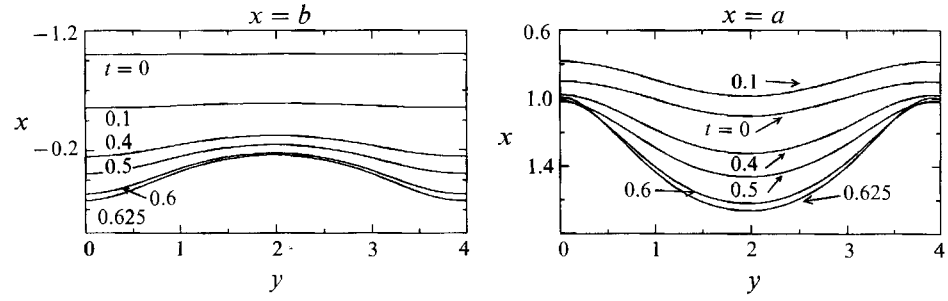

FIGURE 5. The bottom, $x = b$, and top, $x = a$, ridge interfaces at $t = 0$, 0.1, 0.4, 0.5, 0.6, 0.625 for $\hat{A} = 0.1$, $\alpha = \beta = 10$, $V = 2.5$ and $d = 0.625\pi$.

advances down the inclined plane with increasing time while C_a at first contracts to about $x = 0.87$ and then moves down the plane with the spanwise variation decaying with time. This evolution of the ridge is consistent with the linear stability analysis since $Q = 4\sqrt{2} > 1.9987$ and hence we are in a stable regime. From figure 2 we see that the difference between the final values of a and b is approximately $1.41 \approx \sqrt{2} = A_\infty$. Hence the no-spanwise-variation solution (3.10) can be expected to be a good approximation. In particular in figure 3 we plot the value of A at $y = 0$ for the case in figure 2 along with the analytical solution (3.10) with $A_0 = 1.9$. We see that for all time (3.10) is a good approximation to the numerical solution.

In figure 4 we set $d = \frac{1}{2}\pi$ and keep the other parameters the same as in figure 2. We find that $Q = \sqrt{2}$. Thus value of Q is predicted to be unstable from the linear analysis (see I for specifics) and it is very close to the neutral stability curve. We see that as in figure 2 the initial disturbance moves forward along C_b but is retracted along C_a initially. The rate of change is considerably slower for this case but as with the case presented in figure 2 the initial perturbation eventually decays and we find that a stable ridge with no spanwise variation propagates down the plane. Hence this nonlinear case is stable.

In figure 5 we set $d = 0.625\pi$ and again keep the other parameters as in figure 2. Once again the back interface C_b initially advances down the inclined plane while the front interface C_a in initially retracted. This time we see that the regions where $A = a - b$ is the smallest will move with the fastest approach velocity and eventually these regions will touch. Numerically we do not actually see the touching, rather the region becomes very thin. Hence the periodic disturbance along the ridge will form a periodic array of droplets. Our computations end at this critical breaking time. The motion of a droplet along an inclined plane has been studied by others (e.g. Dussan

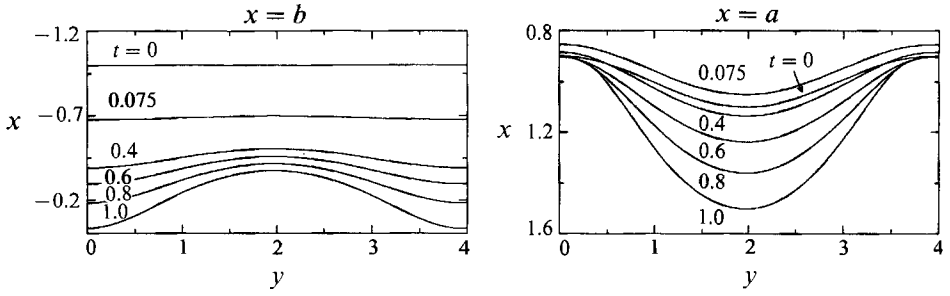

FIGURE 6. The bottom, $x = b$, and top, $x = a$, ridge interfaces at $t = 0$, 0.075, 0.4, 0.6, 0.8, 1.0 for $\hat{A} = 0.1$, $\alpha = 10$, $\beta = 8.5$, $V = 2.5$ and $d = 0.625\pi$.

V. & Chow 1983). Note that $Q = \sqrt{2}/3 < 1.1997$ and hence this situation is linearly unstable.Our calculations show that this instability developed into the breakup of the ridge into droplets. In Huppert's (1982) experiments he noted two types of possible flows of an interface down an inclined plane, the sawtooth interface which coated and the fingering interface which did not coat. Here we find a similar situation. The small-d ridges will coat the plane with the disturbance decaying with time while the large-d ridges will form a periodic array of droplets which will only coat part of the plane. Also the width of the regions coated will depend only on the physical parameters related to the ridge and not to the initial perturbation. Other periodic initial perturbations besides (3.18) were tried in our $2d$-periodic set-up on both C_a and C_b yet we always found that the wavelength of period $2d$ grew most quickly. Hence this nonlinear model does not select the mode of dominant growth but it does describe what happens after the selection is done. Later we shall discuss a linear stability analysis which will select the dominant growth mode.

The effect of varying the other parameters had a similar behaviour and followed the predictions of the linear stability analysis, i.e. if $Q = (\pi/d)(2V/\alpha)^{\frac{1}{2}}$ was large, we found stability while if Q was small the initial perturbation grew and droplets were formed. Hence the larger the static contact angle, the more unstable was the evolution of the ridge. Also large volumes V imply a stable evolution while surface tension will dominate for small volumes and droplets will form.

The linear stability of a steadily moving ridge when there is contact-angle hysteresis was also discussed in I. The result is simply to replace α in the above formula for Q by $\frac{1}{2}(\alpha+\beta)$. Here we wish to discuss the initial-value problem. Suppose we set $\alpha = 10$ and $\beta = 8.5$ with the rest of the parameters the same as in figure 5. The results are shown in figure 6. We see that initially the interface C_a again retracts while C_b is again advancing forward. The rate of advance of C_b is seen to be less than the advance of the case of figure 5, which has no hysteresis. At about $t = 0.075$ the interface C_a stops. Hence the contact angle is now less than α. The back is still advancing and hence fluid begins to collect near the front C_a. At about $t = 0.175$ the front C_a beings to advance down the plane. The middle of C_a moves faster than the sides and as time increases the portion of C_a in the neighbourhood of the sides will stop but the middle will continue to advance. The interface C_b continues to advance down the plane and eventually the regions between C_a and C_b which are closest together will approach each other and droplets will form as expected from the linear stability analysis, since $Q = 0.490$. In figure 7 we set $\beta = 5.0$ and keep the other parameters the same as in figure 6. Here we see that again the interface C_b initially begins to move down the plane but this time the interface C_a does not move. As times

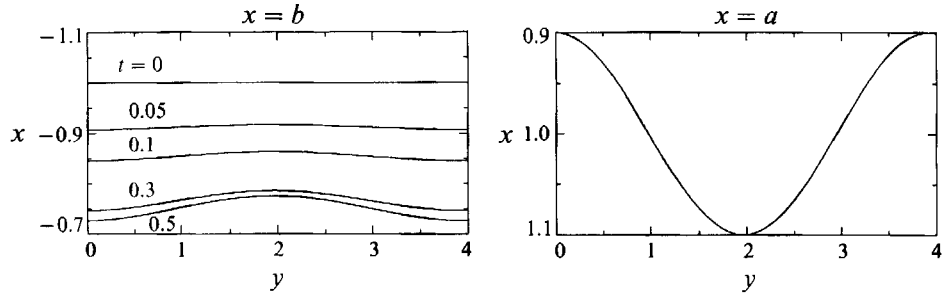

FIGURE 7. The bottom, $x = b$, and top, $x = a$, ridge interfaces at $t = 0$, 0.05, 0.1, 0.3, 0.5 for $\hat{A} = 0.1$, $\alpha = 10$, $\beta = 5.0$, $V = 2.5$ and $d = 0.625\pi$. The interface $x = a$ does not move.

increases the interface C_b approaches an equilibrium position (given approximately by C_b at $t = 0.5$ as illustrated in figure 7). Hence the final solution for the ridge is a steady shape which does not move along the plane. In other words, with hysteresis it is possible to have a static ridge.

4. Linear stability without assuming any contact-angle variation

In §3 the variation of the contact angle as defined outside the immediate vicinity of the contact line was prescribed. As explained in the Introduction, this variation may be assumed to be a property of the materials concerned (Greenspan 1978) or one that can be deduced from the analysis of the slip region near the edge (Hocking 1981). In either case, the angle–velocity relationship introduces a velocity scale and hence a capillary number. But, in the first case, the capillary number is an external parameter and it is legitimate to consider the limit as the capillary number tends to zero, as is done in the quasi-static approximation used in §3 and in I. In the second case, however, the capillary number associated with the angle–velocity relationship is not an assigned parameter but one that must be deduced from the analysis of the slip region near the edge, and its magnitude will depend on the slip length. Hence, in this case, it is necessary to consider more carefully the validity of the quasi-static approximation.

We restrict attention to the linear stability of the ridge, and we attempt to answer two questions. The first is to decide whether or not the model used in §3 is valid under the assumptions of this approach. That is, can we recover the linear stability results for the ridge as obtained by I and so justify the neglect of the slip region. The second question is to determine the relation between a complete solution for the ridge, in which the presence of the contact lines are fully taken into account, with the Troian *et al.* (1989) solution for the instability of the leading edge of an elongating sheet of fluid, in which there was no contact line but a preferred wavelength for the instability was obtained.

The basic state whose stability is to be determined is that of a ridge of fluid in equilibrium. In order to consider a sinusoidal perturbation, we must permit both edges to move in either direction. Hence there can be no contact-angle hysteresis. On the other hand, we do not want to confine our attention to horizontal planes only, so different conditions are needed at the two edges. To achieve this aim, we suppose that the nature of the substrate under the top edge is different from that under the bottom edge, so that the contact angles at the two edges are different but constant. This is, of course, an artificial situation, but the main conclusion that we are trying to establish is expected to apply in more realistic circumstances.

We use the same non-dimensionalization as before, but now we choose the scales a_0 and α_0 so that $V = \frac{3}{4}$ and keep K as a parameter that can take a range of values. We write

$$V' = a_0^2 \alpha_0 d', \quad K = \rho g \sin\theta a_0^2/(\alpha_0 \gamma) = \tfrac{9}{2}k. \tag{4.1}$$

The height h_0 of the ridge in the equilibrium position is given by

$$h_0 = \tfrac{3}{4}(1-x^2) + \tfrac{3}{4}kx(1-x^2), \tag{4.2}$$

and the bottom and top edges are at $a = 1$ and $b = -1$. The slopes at the two edges are then given by

$$-\frac{\partial h_0}{\partial x}\bigg|_{x=1} = \tfrac{3}{2}(1+k), \quad \frac{\partial h_0}{\partial x}\bigg|_{x=-1} = \tfrac{3}{2}(1-k). \tag{4.3}$$

The parameter k must lie in the range $0 \leqslant k \leqslant 1$ for h_0 to be positive between the two edges. We consider for simplicity the special case when there is no hysteresis and, since the ridge is in equilibrium, the (scaled) contact angles are equal to $\frac{3}{2}(1 \pm k)$.

Our objective is to determine the linear stability of this equilibrium state, given that the slopes at each contact line remain constant. The boundary conditions for $h(x, y, t)$ at the upper edge, $x = b(y, t)$, and at the lower edge, $x = a(y, t)$, are

$$h(b, y, t) = 0, \quad h(a, y, t) = 0, \tag{4.4}$$

$$\frac{\partial h}{\partial x}\bigg|_{x=b}\left[1+\left(\frac{\partial b}{\partial y}\right)^2\right]^{\frac{1}{2}} = \tfrac{3}{2}(1-k), \quad -\frac{\partial h}{\partial x}\bigg|_{x=a}\left[1+\left(\frac{\partial a}{\partial y}\right)^2\right]^{\frac{1}{2}} = \tfrac{3}{2}(1+k). \tag{4.5}$$

The volume condition (2.7) now has the form

$$\int_0^d \int_b^a h \, \mathrm{d}x \, \mathrm{d}y = d. \tag{4.6}$$

The equation for h is no longer the quasi-steady one used in §3 but we have to employ the full version (2.1). We make a linear perturbation with wavelength $2\pi/q$ to the height h and to the position of the edges, so that they are given by

$$\left.\begin{aligned} h &= h_0 + \epsilon h_1(x)\cos(qy)\,\mathrm{e}^{\omega t}, \\ \begin{bmatrix} a \\ b \end{bmatrix} &= \begin{bmatrix} 1 \\ -1 \end{bmatrix} + \epsilon \begin{bmatrix} a_1 \\ b_1 \end{bmatrix} \cos(qy)\,\mathrm{e}^{\omega t} \end{aligned}\right\} \tag{4.7}$$

For an unbounded ridge, q can take any value and we can choose $d = \pi/q$; for a ridge of width d, we must have $qd = m\pi$ for some integer m. Substituting these expressions into (2.1) and retaining only the terms of order ϵ, we find that

$$\omega h_1 + h_0^2(h_0+\lambda)(\mathrm{D}^2-q^2)^2 h_1 + h_0(3h_0+2\lambda)\,\mathrm{D}h_0(\mathrm{D}^2-q^2)\,\mathrm{D}h_1 = 0, \tag{4.8}$$

where $\mathrm{D} = \mathrm{d}/\mathrm{d}x$.

The linearized forms of the boundary conditions (4.4) and (4.5) give the conditions

$$h_1(-1) + b_1 \mathrm{D}h_0(-1) = 0, \quad b_1 \mathrm{D}^2 h_0(-1) + \mathrm{D}h_1(-1) = 0, \tag{4.9}$$

$$h_1(1) + a_1 \mathrm{D}h_0(1) = 0, \quad -a_1 \mathrm{D}^2 h_0(1) - \mathrm{D}h_1(1) = 0. \tag{4.10}$$

From the known value of h_0, a_1 and b_1 can be eliminated from these conditions and they can be replaced by the two conditions

$$\mathrm{D}h_1(-1) = -\frac{1-3k}{1-k}h_1(-1), \quad \mathrm{D}h_1(1) = \frac{1+3k}{1+k}h_1(1). \tag{4.11}$$

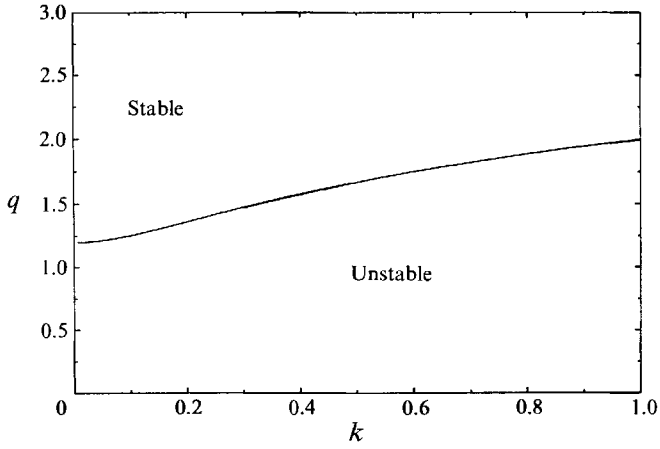

FIGURE 8. Stability diagram in the (q, k)-plane.

The volume condition (4.6) is automatically satisfied unless $q = 0$, in which case we have the condition

$$\int_{-1}^{1} h_1 \, dx = 0. \tag{4.12}$$

This completes the formulation of the eigenvalue problem to determine the possible values of ω. An eigenvalue with a positive real part indicates that the ridge is unstable. Although the equation for h_1 is linear, it is of fourth order and has variable coefficients, so its solution is not simple.

A neutral solution of this problem exists at each value of k if q is chosen appropriately. With $\omega = 0$, the solution of (4.8) for h_1 which does not have a singularity at the edges where h_0 is zero has the form

$$h_1 = A \cosh qx + B \sinh qx, \tag{4.13}$$

where A and B are constants. Note that this solution does not depend on the slip coefficient λ. The boundary conditions (4.11) then show that

$$k^2 = \frac{(1+q^2)\tanh(2q) - 2q}{(9+q^2)\tanh(2q) - 6q}. \tag{4.14}$$

In figure 8 we plot q as a function of k for $0 \leqslant k \leqslant 1$ as given by (4.14) and we label the stable and unstable regions of the (q, k)-plane. Note that the ridge is always unstable for small values of q. Also note that this neutral stability curve is independent of the value of the slip parameter λ. Hence the range of unstable wavenumbers is independent of λ but there can be a different most unstable wavenumber for each λ. The task is to determine the values of q for which the growth rate of the instability is largest.

The linear eigenvalue problem (4.8) and (4.11) can be solved numerically for a given value of q. This is done by discretizing the differential equation (4.8) using a Chebychev pseudo-spectral approximation of the derivatives (see e.g. Canuto *et al.* 1988), and forcing the boundary condition (4.11) at $x = -1$ and the additional condition that $dh_1/dx = 1$ at $x = 1$. The latter is allowed as long as the derivative is non-zero at $x = 1$ since the solution is unknown up to a multiplicative constant. Then for a given value of ω this linear system can be solved for the unknown values of h_1.

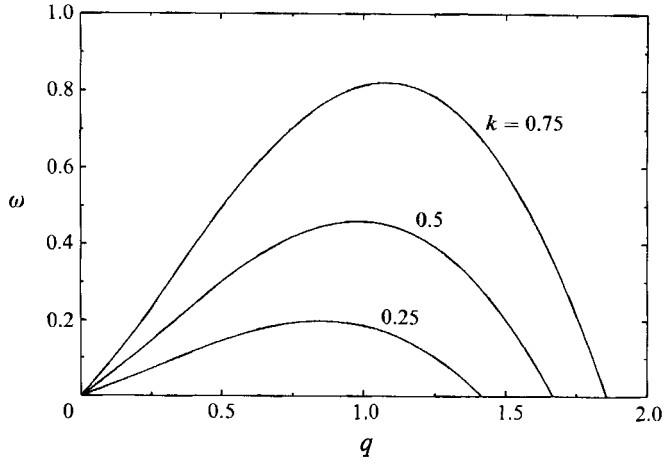

FIGURE 9. Most unstable eigenvalue ω versus the wavenumber q determined from (4.8) and (4.11) for $k = 0.25$, 0.5, 0.75 and $\lambda = 0.01$.

The boundary condition (4.11) at $x = 1$ is then checked and the procedure is repeated for a different guess of ω until the boundary condition (4.11) at $x = 1$ is satisfied to sufficient accuracy.

The advantage of the Chebychev pseudo-spectral approximation is that it gives a very good approximation of the derivatives in the neighbourhood of the contact lines. In order to increase the accuracy in this neighbourhood we have also introduced a stretching of the independent variable $x = \tanh(\hat{\alpha}s)/\tanh(\hat{\alpha})$. Usually $\hat{\alpha}$ was set to 2. We note that the equation is never forced at the contact line itself and hence only h_1 and its first derivative are required there. A local analysis about the contact line (see §5) reveals that h_1 behaves like $(x-1)^2 \ln(1-x)$ in the neighbourhood of the contact line at $x = 1$; a similar behaviour holds near $x = -1$. This implies that the second derivative of h will tend to infinity as we approach the contact line and the numerical method will try to capture this singularity. We find that h_1 and $\mathrm{d}h_1/\mathrm{d}x$ converge very well while the other derivatives tend to infinity there. Since we never force the differential equation at the contact line we are not trying to approximate the infinity and numerical tests indicate a convergence of the height h_1 and its first derivative all along the interval and at the contact line. For a fixed value of x between -1 and 1 we also see convergence of the higher derivatives as we increase the number of collocation points.

In figure 9 we sketch the first eigenvalue ω as a function of the wavenumber q for $k = 0.25$, 0.5 and 0.75 and for $\lambda = 0.01$. We see that, as k increases, the magnitude of the maximum eigenvalue, ω_{m}, increases. The value of q at the maximum ω, say q_{m}, also increases with k but only slightly. Note that k is a measure of the difference between the contact angles at the top and the bottom of the ridge.

Changing the value of the slip parameter has a twofold effect. First it decreases the value of the eigenvalue ω for a given q and secondly it lowers the value of q_{m}. Hence the slip parameter λ does have a significant effect on the preferred wavelength. Unfortunately as we decrease λ we must also increase the number of collocation points in order to get a converged eigenvalue. In particular for $\lambda = 10^{-4}$ we need 320 collocation points in order to get two-decimal-place accuracy. Decreasing λ further requires additional collocation points. Hence an alternative approach is required to solve this eigenvalue problem for very small λ. In §5 we will use an asymptotic

analysis for these small values of λ which together with the numerical solution gives a complete picture of the behaviour of the eigenvalues and in particular the preferred wavenumber for the instability q_m.

These results indicate that there is indeed a preferred wavelength of the instability and to this extent they are parallel to the results Troian *et al.* (1989) for the elongating sheet. In both cases, however, this wavelength is not precisely determined. In the present case it depends logarithmically on the slip coefficient. In Troian's case, it was a weak function of the height of the film that was assumed to extend down the plane ahead of the leading edge of the advancing sheet. Hence the second of the two questions posed in this section has been answered.

There remains the question about the validity of the neglect of the slip region and the consequent failure to predict a preferred wavelength for the instability. This suggests the need for an improved treatment of the slip region. On the other hand, it seems at least plausible that the model of I is correct when the slip region is very small, that is, in the limit as $\lambda \to 0$. The numerical work described in this section could not determine this limiting behaviour, because to find the solution for very small values of λ means that it is necessary to take a very large number of terms in the spectral series. Hence there is a computational limitation in this procedure that prevents the limiting situation from being achieved. The remedy is to analyse the slip region separately from the locations in the width of the ridge where slip can be neglected.

5. Asymptotic solution for $\lambda \to 0$

The eigenvalue problem is specified by (4.8) with h_0 given by (4.2). The two boundary conditions (4.11) are sufficient for the fourth-order equation, since they imply that h_1 and Dh_1 are bounded at the two edges. In this section, we take q and k to be $O(1)$ as $\lambda \to 0$ and find the asymptotic value of ω. We first consider inner regions of width λ at both edges.

If we write $x = 1 - \lambda\xi$, the static solution (4.2) for h_0 when ξ is of order one becomes

$$h_0 = \tfrac{3}{2}(1+k)\lambda\xi + O(\lambda^2), \tag{5.1}$$

and the solution for h to order λ can be written as

$$h = 1 - \frac{1+3k}{1+k}\lambda\xi - \frac{8\lambda\omega}{27(1+k)^3} f(\xi), \tag{5.2}$$

where

$$\frac{d^3 f}{d\xi^3} = \frac{1}{\xi\left[\xi + \dfrac{2}{3(1+k)}\right]}, \quad \frac{df}{d\xi} = 0 \quad \text{at} \quad \xi = 0, \qquad f = o(\xi^2) \quad \text{as} \quad \xi \to \infty. \tag{5.3}$$

Because the boundary condition (4.11) is homogeneous, any multiple of this solution is permissible. If we integrate three times to determine f and find the asymptotic form of the solution as $\xi \to \infty$, we can apply a matching principle to show that the outer solution as $x \to 1$ must be a multiple of

$$h_+ \sim 1 - \frac{1+3k}{1+k}(1-x) - \frac{8\omega}{27(1+k)^3}(1-x)\left\{\ln(\lambda) - \ln(1-x) + \ln\left[\frac{2}{3(1+k)}\right]\right\}, \tag{5.4}$$

neglecting terms $O(\lambda \ln \lambda)$. In the same way we can show that the outer solution as

$x \to -1$ must be a multiple of h_-, which can be found from h_+ by changing the signs of k and of x whenever they occur in (5.4).

In the outer region x is of order one, and (4.8) to leading order in λ can be written as a pair of coupled equations of the form

$$\mathrm{D}(h_0^3\,\mathrm{D}G) - q^2 h_0^3 G + \omega H = 0, \quad \mathrm{D}^2 H - q^2 H = G, \tag{5.5}$$

where $\mathrm{D} = \mathrm{d}/\mathrm{d}x$ and h_0 is given in (4.2). The boundary conditions are provided by (5.4) for h_+ and its companion form for h_-. Thus, as $x \to 1$,

$$\left.\begin{aligned} H &= c_+, \\ \mathrm{D}H &\sim c_+ \left\{ \frac{1+3k}{1+k} - \frac{8\omega}{27(1+k)^3}\left[\frac{1}{\epsilon} + \ln\frac{3(1+k)}{2} + 1 + \ln(1-x) \right] \right\}, \\ G &\sim c_+ \frac{8\omega}{27(1+k)^3}\frac{1}{1-x}, \end{aligned}\right\} \tag{5.6}$$

and, as $x \to -1$,

$$\left.\begin{aligned} H &= c_-, \\ \mathrm{D}H &\sim -c_- \left\{ \frac{1-3k}{1-k} - \frac{8\omega}{27(1-k)^3}\left[\frac{1}{\epsilon} + \ln\frac{3(1-k)}{2} + 1 + \ln(1+x) \right] \right\}, \\ G &\sim c_- \frac{8\omega}{27(1-k)^3}\frac{1}{1+x}, \end{aligned}\right\} \tag{5.7}$$

where

$$\epsilon = 1/|\ln\lambda| \ll 1, \quad 0 \leqslant k < 1, \quad q \geqslant 0. \tag{5.8}$$

Our objective is to determine the eigenvalue ω as a function of k and q for small values of ϵ.

Because there is no longer any necessity to resolve the regions of order λ near the two edges, the numerical solution of (5.5) is much simpler than that of (4.8) when λ is small enough for ϵ to be regarded as a small quantity. At the edges, G and D^2H are singular, but H and $h_0^3\,\mathrm{D}G$ are not singular there. We will solve (5.5) by applying the same Chebychev pseudo-spectral method as described in §4. Since the boundary conditions (5.6) and (5.7) are a result of the matching principle we will apply them at a fixed but small distance, δ, from the boundaries. Hence the interval where (5.5) holds is smaller and we map it onto $[-1, 1]$ using the change of independent variable $s = x/(1-\delta)$. Then following the numerical method outlined in §4 we force at $s = -1$ the boundary conditions (5.7) to hold while at $s = 1$ we set $H = 1$ and require the condition on the first derivative of H in (5.6) to hold. The eigenvalue ω is determined by checking to see if the condition on the second derivative in (5.6) is satisfied at $s = 1$. Since there were no longer any singularities at the end points of the computational domain this method converged very well as the number of collocation points increased. For example, for $k = 0.5$, $\delta = 0.01$, $q = 0.975$ and for $\lambda = 0.01$ we find that the new asymptotic method predicts that $\omega = 0.445$ for 40 collocation points while the method of §4 predicts $\omega = 0.451$ (here we set $\hat{\alpha} = 2$). The converged result is $\omega = 0.446$ to three decimal places. If we set $\lambda = 0.0001$ and keep the other parameters the same we find that again for 40 collocation points the asymptotic method gives $\omega = 0.332$, the converged result, while the calculation of §4 gives $\omega = 0.377$. As λ decreases, more and more collocation points are necessary for the method of §4 while the numerical accuracy of the asymptotic method is only weakly dependent on λ. We should note that the correct answer must be independent of δ

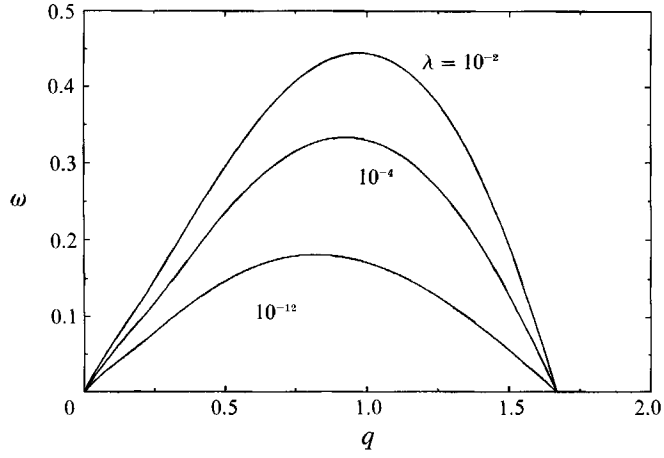

FIGURE 10. Most unstable eigenvalue ω versus the wavenumber q determined from (5.5)–(5.7) for $\lambda = 10^{-2}$, 10^{-4}, 10^{-12} and $k = 0.5$.

but clearly this method is dependent on the distance parameter δ and hence an error is introduced. This error tends to zero as δ tends to zero, so we need to select δ sufficiently small. Through a series of numerical tests we have found that setting $\delta = 0.01$ gives graphical accuracy over a wide range of λ using 40 collocation points. In figure 10 we plot the eigenvalue ω as a function of the wavenumber q for $k = 0.5$ and $\delta = 0.01$. We note that ω_m and q_m both decrease with decreasing λ. Also as noted in figure 8 the unstable range of values of q is independent of λ.

The solutions of (5.5) for small values of ϵ posed no particular difficulty, and it was found that the value of ω was approximately proportional to ϵ and then that ω had a maximum as a function of q, with $\omega = 0$ when $q = 0$. On the other hand, we can consider the asymptotic solution of (5.5) for small ϵ. In this limit, $G = 0$ and

$$H = A\cosh qx + B\sinh qx, \tag{5.9}$$

and the boundary conditions (5.6) and (5.7) then give an equation for $\Omega = 8\omega/27\epsilon$ in the form

$$\Omega^2\tanh(2q) + 2\Omega\{q(1+3k^2) - (1+7k^2)\tanh(2q)\} + (1-k^2)^2\tanh(2q)\{q^2(1-k^2)+1-9k^2\} - 2q(1-k^2)^2(1-3k^2) = 0. \tag{5.10}$$

This equation is similar to that found in I when the presence of the edge regions was represented by an assumed velocity-dependent variation of the contact angle outside these regions. There is instability for all q less than a critical value that is a function of k. This is determined by setting Ω to zero and we then recover (4.14). Also, we note that Ω has a maximum value Ω_c when $q = 0$, where Ω_c is the positive root of the equation

$$\Omega^2 - (1+11k^2)\Omega - 6k^2(1-k^2)^2 = 0. \tag{5.11}$$

This limiting behaviour as $\epsilon \to 0$ was not obtained by the numerical solution for a small value of λ in §4, but the solutions of (5.5) for small ϵ do confirm that ω is $O(\epsilon)$.

In order to remove the discrepancy between the numerical solutions for small ϵ and the asymptotic limit as $\epsilon \to 0$, we consider the solution of (5.5) when both ϵ and q are small. If we write $\omega = 27\epsilon\Omega/8$ and $q = \epsilon^{\frac{1}{2}}Q$, the equations (5.5) become

$$\mathrm{D}(h_0^3\,\mathrm{D}G) - \epsilon Q^2 h_0^3 G + \tfrac{27}{8}\epsilon\Omega H, \quad \mathrm{D}^2H - \epsilon Q^2 H = G. \tag{5.12}$$

If we expand G and H in powers of ϵ and write $G = G_0 + \epsilon G_1 + \ldots$, $H = H_0 + \epsilon H_1 + \ldots$, the leading-order solution is

$$G_0 = 1, \quad H_0 = \tfrac{1}{2}(x^2 - 1) + \tfrac{1}{2}(c_1 - c_2)\,x + \tfrac{1}{2}(c_1 + c_2), \tag{5.13}$$

and the boundary conditions (5.6) and (5.7) to this order give the equations

$$c_1\left[\frac{1+3k}{1+k} - \frac{1}{2} - \frac{\Omega}{(1+k)^3}\right] + \frac{c_2}{2} = 1, \tag{5.14}$$

$$c_2\left[\frac{1-3k}{1-k} - \frac{1}{2} - \frac{\Omega}{(1-k)^3}\right] + \frac{c_1}{2} = 1. \tag{5.15}$$

The equation for G_1 is

$$\mathrm{D}(h_0^3\,\mathrm{D}G_1) - Q^2 h_0^3 G_0 + \tfrac{27}{8}\Omega H_0 = 0. \tag{5.16}$$

From the boundary conditions on G_1 given in (5.6) and (5.7), it follows that $H_0^3\,\mathrm{D}G_1 = 0$ at $x = \pm 1$, so we can integrate (5.16) to obtain

$$Q^2 \int_{-1}^{1} h_0^3 G_0\,\mathrm{d}x = \tfrac{27}{8}\Omega \int_{-1}^{1} H_0\,\mathrm{d}x. \tag{5.17}$$

When the known values of h_0, G_0 and H_0 are substituted into this equation together with the values of c_1 and c_2 determined from (5.14) and (5.15), we obtain an equation for Q as a function of Ω and k in the form

$$Q^2 = \frac{35\Omega^2}{2(3+k^2)}\left[\frac{2(1-k^2)+\Omega}{6k^2(1-k^2)^2 + \Omega(1+11k^2) - \Omega^2}\right]. \tag{5.18}$$

This equation shows that, as $Q \to 0$, $\Omega \sim Q$ and as $Q \to \infty$, $\Omega \to \Omega_c$. In terms of the unscaled variables, this means that, for small values of $q/\epsilon^{\frac{1}{2}}$,

$$\omega \sim \frac{81}{4\sqrt{70}}\, k\{(1+\tfrac{1}{3}k^2)\,(1-k^2)\,\epsilon\}^{\frac{1}{2}} q, \tag{5.19}$$

and, as $q/\epsilon^{\frac{1}{2}} \to \infty$, $\omega \to \frac{27}{8}\epsilon\Omega_c$, which agrees with the limiting value of ω as $q \to 0$ found from (5.10).

It follows that, as $\epsilon \to 0$, there is a maximum growth rate of the instability of order ϵ, but this occurs when the wavenumber q is of the order $\epsilon^{\frac{1}{2}}$. The method of I is correct in the limit as the slip length tends to zero, but absurdly small values must be chosen if the limiting solution is to be obtained numerically. If $q = 0.1$, we must take ϵ of order 10^{-2} and then λ is of order 10^{-43}. The analysis and the numerical results in §4, which predict a preferred growth rate at a wavenumber that is not small, are seen to be true, provided that the chosen value of λ is not so small that $\epsilon = 1/|\ln\lambda|$ is also small.

6. Conclusions

The first part of this paper has examined the nonlinear development of a perturbation to the positions of the edges of a ridge of fluid sliding down an inclined plane. The numerical solutions were based on the quasi-steady hypothesis and assumed that the influence of the regions close to the contact lines on the flow outside them could be represented by assuming a dynamic variation of the contact angle. Although the linear solution based on this assumption predicts an instability of the

edge positions, the maximum growth occurs when the wavenumber is as small as possible. The nonlinear numerical solution, however, showed that, in the unstable region, there was a lateral transfer of fluid into lobes that grew in size, while the depleted portions shrunk until the leading and trailing edges made contact.

In the second part, the quasi-steady assumption was not assumed and the basic assumption concerning the regions near the contact lines was replaced by taking the dynamics in these regions fully into account. With a model that includes a slip region, but without assuming any variation in the contact angle, it was shown that it was possible to replace these regions by suitable boundary conditions. This is, of course, precisely what was done in the first model, but the key difference is that the relevant parameters in the boundary conditions to be imposed is ϵ rather than λ, where λ is the slip length and $\epsilon = 1/|\ln \lambda|$. We have shown that the first model is correct in the limit $\epsilon \to 0$, but that this limit is not approached with any reasonable choice of λ. The second model requires λ to be small, but the numerical value of ϵ can be of order one. Because the solution depends on the value of ϵ, it is important to consider the slip regions in order to establish the way in which the replacement boundary conditions depend on ϵ. We should note that other slip models were considered and similar results were found. It is expected that similar conclusions will follow if a slip-velocity – contact-angle relation were assumed at the contact line in place of the fixed-angle assumption. Hence the quasi-steady assumption, which neglects the effect of viscous forces in the outer region, can be recovered in the limit as ϵ tends to zero and is responsible for the difference between I and the linear stability results presented here.

This work was supported in part by a NATO grant for international collaboration in research. Also M.J.M. was supported in part by DOE grant DE-FG02-88ER13927. M.J.M. wishes to thank Dr G. B. McFadden for several helpful discussions. We are grateful for the comments of a referee, which have helped us to clarify some of the assumptions made in this paper.

REFERENCES

Canuto, C., Hussaini, M. Y., Quarteroni, A. & Zang, T. A. 1988 *Spectral Methods in Fluid Dynamics*. Springer.

Dussan V., E. B. & Chow, R. T-P. 1983 On the ability of drops and bubbles to stick to non-horizontal surfaces of solids. *J. Fluid Mech.* **137**, 1–29.

Greenspan, H. P. 1978 On the motion of a small viscous droplet that wets a surface. *J. Fluid Mech.* **84**, 125–143.

Greenspan, H. P. & McCay, B. M. 1981 On the wetting of a surface by a very viscous fluid. *Stud. Appl. Maths* **64**, 95–112.

Haley, P. J. & Miksis, M. J. 1991 The effect of the contact line on droplet spreading. *J. Fluid Mech.* **223**, 57–81.

Hocking, L. M. 1981 Sliding and spreading of thin two-dimensional drops. *Q.J. Mech. Appl. Maths* **34**, 37–55.

Hocking, L. M. 1990 Spreading and instability of a viscous fluid sheet. *J. Fluid Mech.* **211**, 373–392 (referred to herein as I).

Hocking, L. M. 1992 Rival contact-angle models and the spreading of drops. *J. Fluid Mech.* **239**, 671–681.

Huppert, H. E. 1982 Flow and instability of viscous gravity currents down a slope. *Nature* **300**, 427–429.

Longuet-Higgins, M. S. & Cokelet, E. D. 1976 The deformation of steep surface waves on water I. A numerical method of computation. *Proc. R. Soc. Lond.* A **350**, 1–26.

MIKSIS, M. J., VANDEN-BROECK, J.-M. & KELLER, J. B. 1981 Axisymmetric bubble or drop in a uniform flow. *J. Fluid Mech.* **108**, 89–100.

SILVI, N. & DUSSAN, V., E. B. 1985 On the rewetting of an inclined solid surface by a liquid. *Phys. Fluids* **28**, 5–7.

TROIAN, S. M., HERBOLZHEIMER, E., SAFRAN, S. A. & JOANNY, J. F. 1989 Fingering instabilities of driven spreading films. *Europhys. Lett.* **10**, 25–30.

TUCK, E. O. & SCHWARTZ, L. W. 1990 A numerical and asymptotic study of some third-order ordinary differential equations relevant to draining and coating flows. *SIAM Rev.* **32**, 453–469.